ELSEVIER

Contents lists available at ScienceDirect

Materials Science & Engineering C

journal homepage: www.elsevier.com/locate/msec



Novel PMMA bone cement nanocomposites containing magnesium phosphate nanosheets and hydroxyapatite nanofibers



Abhijit H. Phakatkar^a, Mostafa Rezazadeh Shirdar^b, Mei-li Qi^{c,d}, Mohammad Mahdi Taheri^b, Surya Narayanan^b, Tara Foroozan^a, Soroosh Sharifi-Asl^a, Zhennan Huang^a, Megha Agrawal^b, Yu-peng Lu^c, Reza Shahbazian-Yassar^{a,*}, Tolou Shokuhfar^{b,*}

- ^a Department of Mechanical and Industrial Engineering, University of Illinois at Chicago, Chicago, IL 60607, USA
- ^b Department of Bioengineering, University of Illinois at Chicago, Chicago, IL 60607, USA
- ^c School of Jiaotong and Civil Engineering, Shandong Jiaotong University, Ji'nan 250357, China
- ^d School of Materials Science and Engineering, Shandong University, Ji'nan, 250061, China

ARTICLE INFO

Keywords: PMMA nanocomposite Two-dimensional magnesium phosphate nanosheets HA nanofibers Compressive strength Antibacterial property Bioactivity Cytotoxicity

ABSTRACT

Lack of bioactivity and monomer toxicity are limiting factors of polymethyl methacrylate (PMMA) bone cement in orthopedic applications. Herein, we address these shortcomings by proposing two-dimensional magnesium phosphate (MgP) nanosheets and hydroxyapatite (HA) nanofibers as novel fillers in PMMA bone cement nanocomposites. Two-dimensional MgP nanosheets and one-dimensional HA nanofibers were synthesized by tuning the crystallization of the sodium-magnesium-phosphate ternary system and hydrothermal homogeneous precipitation, respectively. We show that MgP nanosheets exhibit antibacterial properties against *Escherichia coli* (*E. coli*). In addition, HA nanofibers with high level of bioactivity are the proper choice to induce cell viability in the nanocomposite. Results indicate that the combination of both fillers can act as deformation locks enhancing the compressive strength of the nanocomposites. The synthesized nanocomposite possesses excellent bioactivity, mechanical properties, and cytocompatibility potentially opening new paradigm in the design of next generation bone cement composites.

1. Introduction

Since 1930 polymethyl methacrylate (PMMA) has been used for odontology and subsequently for bone cement material in orthopedic applications [1]. Nowadays, PMMA are used as a grouting material in joint replacement surgeries to transfer the load between the prosthetic implant and the bone [2]. Even though PMMA is widely used as bone cement materials in joint replacement surgeries, several complications such as loosening and secondary fracture of adjustment vertebral bodies have been reported due to the inadequate mechanical and biological properties [3-5]. For instance, monomer toxicity and low level of bioactivity are considered as two disadvantages of the PMMA which limit its clinical uses [6-8]. Furthermore, PMMA is a bioinert material [9] that prevent chemical bonding or osteointegration with the bone tissue at the implant site [10]. This results in weak bonding strength between the bone cement and the host bone [11]. It was reported that such weak bonding may cause micro motion in daily activity, which then can lead to the formation of small wear debris resulting in osteolysis and further aseptic loosening or even dislodgement of the bone cement implant [12].

The enhancement of the PMMA-based bone cement properties is a challenging issue that has been the focus of much research. Application of filler materials into the matrix of PMMA has been considered as a potential solution to improve its properties and overcome the limitations. The studies of Kwon and co-workers showed that incorporation of 30 wt% hydroxyapatite (HA, Ca₁₀(PO₄)₆(OH)₂) in PMMA-HA composite increased the interfacial shear strength at the bone implant interface after six weeks of implantation [13]. Recently, the nanomechanical behavior of individual HA nanofibers were directly visualized using in situ TEM methods for the first time by our group [14]. The nanofibers can be severely scrolled and stretched through several cyclic compression tests without damage, showing remarkable nanomechanical flexibility, which supports HA nanofibers to be used as a filler in biomedical composite materials. In addition, Moursi et al. [15] reported that the addition of HA in a PMMA matrix improves osteoblast response as compared to PMMA alone. The use of micro and nano scales alumina fillers for improvement of the mechanical properties of hybrid PMMA composites was also reported by Faisal et al. [16]. Owing to the special

E-mail addresses: rsyassar@uic.edu (R. Shahbazian-Yassar), tolou@uic.edu (T. Shokuhfar).

^{*} Corresponding authors.

properties of materials in nanoscale, the incorporation of nano-sized materials has been widely explored as potential solutions to improve the mechanical properties of PMMA [17]. Multiwalled carbon nanotube [18,19], graphene [17] calcium carbonate nanoparticles [20], collagen [5], silica nanoparticles [21], core-shell nanoparticles [22] and $\rm ZrO_2$ nanotubes [23] are some examples of such materials that have been added to PMMA to boost its properties.

Development of bacteria resistance bone cement is also an interesting challenge for many researchers. PMMA by itself not only does not have antibacterial properties [24], but also is very susceptible to bacterial adhesion and colonization [25]. Therefore, silver and gold nanoparticles were added to the PMMA-based bone cement to provide robust antibacterial properties [26-29]. However, the toxicity of silver and gold is still a matter of concern [30,31]. Incorporation of antibiotics directly into PMMA has been reported as the second method to prevent infection, however, there are several drawbacks associated to this method which reduce the success rates [32]. Recently, incorporation of nano-additives in the form of nanospheres, nanosheets, nanofibers, or nanotubes is one of the most intriguing approaches to improve antibacterial properties of PMMA [33]. Magnesium phosphate has been demonstrated to be a biocompatible material in vivo making it interesting for biomedical applications [34]. Magnesium ions from magnesium phosphates can catalyze various enzymes and can enhance cells proliferation [35,36]. The dissolution by-products released from magnesium phosphate are mainly Mg2+ ions and HPO42-, which completely biocompatible [37]. Recently, thin two-dimensional (2D) layer materials such as two-dimensional MgP nanosheets with desirable biocompatibility, bioresorption, and long-term stability have been attracting extensive interest in biomedical applications [38].

Developing PMMA-based composites with high level of cytocompatibility, mechanical and antibacterial properties is a challenging task. We have designed a PMMA nanocomposite that contain two-dimensional MgP nanosheets and one-dimensional HA nanofibers. We observed that incorporation of these nanofillers could provide an antibacterial PMMA bone cement nanocomposite with high level of cytocompatibility and mechanical properties. The findings of this work reveal that the excellent performance of the proposed bone composite can result in a paradigm shift in design of state-of-the art bone cement composites.

2. Material and methods

2.1. Synthesis of two-dimensional MgP nanosheets

Two-dimensional MgP was synthesized based on the study reported by Laurenti et al. [37]. In brief, the ternary system of NaOH – Mg(OH) $_2$ – $\rm H_3PO_4$ was employed to synthesize MgP. Two precursors of NaOH and $\rm H_3PO_4$ were prepared with 1.5 M concentration. First, the MgOH was dissolved with magnetic stirrer in $\rm H_3PO_4$ until fully clear solution obtained. Then the NaOH solution was added and stands for 2 h. Finally, the prepared solution was centrifuged at 4000 rpm for 5 min and the supernatant was discarded. The molar ratio of MgOH, NaOH and $\rm H_3PO_4$ were adjusted to 0.18, 0.45 and 0.37, respectively. The solid precipitate was vacuum dried at 70 °C for 24 h.

2.2. Synthesis of HA nanofibers

First, aqueous solution of $Ca(NO_3)_2\cdot 4H_2O$, $(NH_4)_2HPO_4$ and 1 M urea solution with the molar ratio of Ca/P kept at 1.67. Then the pH value of the mixed solution was adjusted to 3.50 by using 0.5 M $HNO_{3(aq)}$, and the solution was transferred to a Teflon-lined cylindrical stainless-steel autoclave and treated at 160 °C for 6 h. At last, the products were washed with deionized water and ethanol, and dried in oven at 80 °C [38].

Table 1Classification of specimens in this study.

Samples	Powder (wt%)					
	PMMA	2-D MP	НА			
P	100	0	0			
PM	90	10	0			
PH	90	0	10			
PMH 1	90	7.5	2.5			
PMH 2	90	5	5			
РМН 3	90	2.5	7.5			

2.3. Nanocomposites preparation

The samples were classified into six types (P, PM, PH, PMH1, PMH2, PMH3) based on the ratio of MgP nanosheets and HA nanofibers in PMMA matrix (Table 1). The highest amount of filler ratios was set to 7.5 wt% to ensure a lower degree of agglomeration. To prepare the nanocomposites, methyl methacrylate (MMA) was used as solvent for PMMA. The ratio of PMMA/MMA was set to the 1.52 g/ml [7]. The prepared PMMA-MgP-HA nanocomposite samples were then dried in vacuum for 3 days. In order to dry any remaining liquid, the nanocomposite was oven-dried at 40 °C for 24 h.

2.4. Compression tests

The compression test was conducted in accordance with ISO 5833 standard [39]. Cylindrical specimens with the length of 12.0 \pm 0.1 mm and diameter of 6.0 \pm 0.1 mm were tested under compressive loading using a INSTRON–8500R universal testing machine. The machine operated at a crosshead speed of 2.54 mm/min until specimen failure. The compressive strength was subsequently calculated from the load versus deformation data.

2.5. Antibacterial tests

To culture the bacteria, first the medium was prepared by mixing the LB Broth powder in 500 ml of molecular biology grade water. The solution was stirred for 15 min. The flask containing 50 ml of prepared solution was autoclaved for at 125 °C for 30 min. Thereafter, the mixture was cooled under UV light to be ready as medium for culturing bacteria. The frozen E. coli bacteria were added to the prepared solution. The solution was shaken at 37.5 °C for 16 h to promote the bacterial growth. To prepare the agar plate for conducting inhibition zone evaluation, the LB Agar powder, LB Broth powder and molecular biology grade water were mixed with concentration of 37 g/L. the mixture was stirred for 20 min and then autoclaved. After cooling process, the viscous prepared solution was poured into the petri dishes and wait till solidify. The cultured E. coli bacteria were spread on the solidified agar medium with the help of inoculating loops. Finally, the samples were placed into the center of petri dishes and stored in the incubator at 37.5 °C. The inhibition zones of the samples were observed and imaged after 6, 12, and 24 h.

2.6. Immersion tests

The Simulated Body Fluid (SBF) was prepared with the chemical composition listed in Table 2 with the pH of 7.25. The disk shape specimens of control (P) and nanocomposites (PH, PM, PMH 1, PMH 2, PMH 3) in triplicates with 6 mm diameter and 2 mm length (6 mm \times 2 mm) were immersed into the 50 mL SBF for 10 days. All samples were evaluated at time intervals of 1, 2, 4, 8, 12 h and every day after immersion. The immersion test was conducted in the water bath at 37 °C and the surface area of composite to the volume of SBF was adjusted to 7.5 mm²/ml.

Table 2Chemical composition of the Kokubo simulated body fluid (SBF) compared to the blood plasma [40].

Solution	Ion concentration (mmol/L)								
	Na ⁺	K ⁺	Ca ²⁺	Mg ²⁺	HCO ₃	Cl-	HPO ₄ ²⁻	SO ₄ ²⁻	
Plasma Kokubo (SBF)			2.5 2.5		27.0 4.2	103.0 147.8		0.5 0.5	

2.7. Cytotoxicity tests

In this study, MTT assay method was used for evaluation of cytotoxicity. First, fibroblasts cells (NIH/3 T3 (ATCC® CRL1658)) were cultured in Dulbecco's modified eagle medium (DMEM) with addition of 10% fetal bovine serum (FBS) and 1% penicillin streptomycin and incubated at 37 °C with 5% $\rm CO_2$ and 95% humidity. The disk shape specimens of control (P) and composites (PH, PM, PMH 1, PMH 2, PMH 3) in triplicates with 6 mm diameter and 2 mm length (specimen weight: ~ 50.2 mg) were placed in 96-well plate. Cultured cells at a density of 6×10^5 cells/ml were then seeded on to the specimens with the concentration of 10,000 cells/well (150 μ l final cell media volume per well) followed by incubation for 24 h. In the next step, MTT solution was added and the well-plate was incubated for 4 h. Afterward, dimethyl sulfoxide (DMSO) solvent was added to each well to solubilize formazan salts. Finally, absorption was measured by a microplate reader (Synergy™ H1, BioTek) at 570 nm wavelength.

2.8. Structural and chemical characterizations

In this study, phase composition and crystal structure were evaluated using Bruker D8 Discover X-ray diffractometer (XRD). The nanostructure and elemental analysis of two-dimensional MgP nanosheets and HA nanofibers were observed under scanning transmission electron microscopy (STEM) (JEOL JEM-ARM200CF), field emission scanning electron microscope (FESEM) (JEOL JSM-6320F) and scanning electron microscope (SEM) (Hitachi S-3000 N VPSEM) equipped with energy-dispersive X-ray spectroscopy (EDS).

2.9. Statistical analysis

The obtained data are expressed as mean \pm standard deviation. The experiments were repeated for three times and all comparisons have been made at 95% confidence level. All data were statistically analyzed with One-way ANOVA technique. The statistical significance between sample groups was evaluated by Bonferroni-Holm corrected method (p < .05).

3. Results and discussion

Fig. 1 (a, b) illustrates X-ray diffraction patterns of MgP nanosheets and HA nanofibers, respectively. It can be seen that the diffraction peaks of 2D MP nanosheets (Fig. 1 (a)) made with sodium are mainly composed of Mg₃(PO₄)₂, Na₂HPO₄.2H₂O, Mg₂PO₄(OH), Na₂Mg₅(PO₄)₄.7H₂O. In Fig. 1 (b), all the peaks can be indexed to HA (JCPDS 09–0432) and no other phase was detected indicating that the product is pure HA. This result is in close agreement with the finding of Qi et al. [38].

The morphology, structure, and composition of synthesized two-dimensional MgP nanosheets is shown in Fig. 2. The FESEM and TEM images of two-dimensional MgP nanosheets are illustrated in Fig. 2 (a, b). From these images, it can be inferred that the MgP nanostructures possess sheet-like morphologies of variable dimensions. It contains several ultrathin layers of aggregated and crumpled sheets which formed a continuous network at nanoscale. To confirm the elemental composition of MgP nanosheets, EDS analysis was employed (Fig. 2 (c,

d)). The data confirms that the MgP nanosheets consist of O, C, P, Mg, and Na elements [41]. In addition, the EDS mapping also indicates a homogenous distribution of elements in the nanosheets.

The fiber morphology of synthesized HA nanofibers under a hydrothermal process at pH of 3.5 is illustrated in FESEM and TEM images in Fig. 3 (a, b). The morphology evaluation revealed the formation of solid and uniform HA nanofibers with a random orientation. HA nanofibers are formed in a long length with small diameter. It was reported that there are several requirements for optimal fiber filler in a polymer-based composites [19]. The cross-section area of the fiber should be as small as possible, and the length of the fiber should be long enough to significantly decrease the developed stress within them as compared to the nominal stress of the composite. In addition, the spatial arrangement of the fibers in the matrix needs to be in a specific order to ensure a unidirectional, maximal reinforcement. Therefore, it seems that these HA nanofibers possibly fulfill the requirements of optimal fibers in nanocomposites. The elemental composition of nanofibers determined by EDS spectra analysis (Fig. 3 (c, d)) clearly reveals the existence of Ca, P and O elements in the nanofibers and is in accordance with the XRD results in Fig. 1 (a). In addition, the EDS mapping illustrates a homogeneous distribution of Ca, P, and O elements throughout the fibers.

Fig. 4 (a) shows the schematic diagram for developing PMMA-MgP-HA nanocomposites in this study. From SEM images in two different magnifications (Fig. 4(b)), it is clearly observed that MgP nanosheets and HA nanofibers were homogenously dispersed into the PMMA matrix with the chemical formula of $(C_5O_2H_8)_{n\cdot}$ Incorporation of these two fillers with their specific physical properties into the PMMA matrix fills up the porosity of the matrix and consequently creates a denser nanocomposite structure. EDS spectra and EDS mapping mode of the synthesized nanocomposite is shown in Fig. 4 (c). It confirms that the PMMA-MgP-HA nanocomposite consists of O, C, Mg, P, Ca, and Na elements with a homogenous distribution throughout the nanocomposite.

In the current study, to evaluate the mechanical strength upon addition of MgP nanosheets and HA nanofibers in the PMMA bone cement matrix, the compressive strength was evaluated. The stabilization of the bone cement matrix avoids any possible crack formation by assuring the integrity at bone cement-prosthesis interfaces [41]. The stress-strain curve and ultimate compressive strength of the control and composite samples are shown in Fig. 5 (a). As represented in Fig. 5 (b), the compression strength of P, PM and PH specimens are 30, 49 and 38 MPa, respectively. The statistical data significance was evaluated for with One-way ANOVA followed by the Bonferroni-Holm correction for p < 0.05. The enhanced ultimate strength was observed for all nanofillers integrated PMMA samples (PH, PM, PMH1, PMH2, PMH3) as compared with control PMMA bone cement composite sample. The results (Fig. 5(b)) indicates that the incorporation of 10 wt% of MgP nanosheets and 10 wt% of HA nanofibers into PMMA matrix enhanced the ultimate compressive strength of control PMMA bone cement composite up to 53% and 21%, respectively. It means that both nanofibers and 2D nanosheets possibly act as a deformation lock either in extensional or shear mode which improved mechanical compressive strength. The compression strength of PMH1, PMH2 and PMH3 nanocomposite samples are 58, 56 and 52 MPa respectively. The results therefore indicated that the maximum ultimate compressive strength belongs to the PMMA nanocomposite with optimum concentrations of combined nanofillers as 7.5 wt% MgP nanosheets and 2.5 wt% HA nanofibers. However, with the increase of HA nanofibers ratio to the 5 wt % and 7.5 wt% the compression strength gradually decreases. It appears that increasing the amount of HA nanofibers > 2.5 wt% could possibly results into the agglomeration hence decreasing the homogeneity of bone cement composite matrix that can eventually decrease the compressive strength by promoting the formation of internal cavities and voids [19]. We expect that there would be some degree of chemical bonding among PMMA, MgP nanosheets and HA nanofibers in

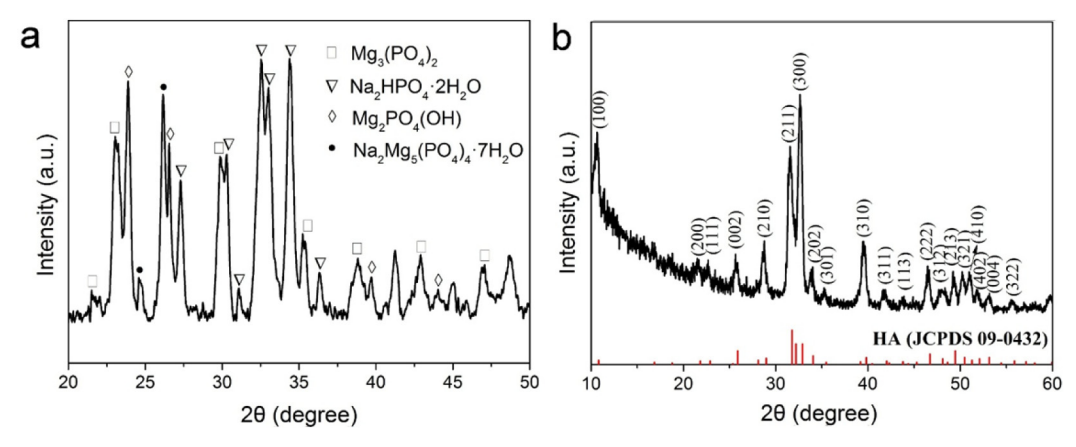


Fig. 1. X-ray diffraction patterns of (a) MgP nanosheets ($2\theta = 20-50$ degree) (b) HA nanofibers ($2\theta = 10-60$ degree). The red-colored peaks in (b) indicates the standard HA from JCPDS 09–0432. (For interpretation of the references to colour in this figure legend, the reader is referred to the web version of this article.)

nanocomposite, which needs to be investigated in future research. Further iterative studies are required to investigate setting time of novel PMMA-MgP-HA bone cement upon integrating with nanofillers at various weight percent in the PMMA bone cement matrix. The artificial aging studies of PMMA-MgP-HA bone cement composites evaluating the degradation of bone cement in bio-chemical environment under the influence of mechanical stresses can provide future directions for in vivo experimentation.

Fig. 6 shows antibacterial activities of the control and nano-composite samples determined by disc-diffusion test against *E. coli* bacteria after 24 h. It is clear that there is no inhibition zone for PMMA sample (Fig. 6 (a)), which indicates that PMMA by itself does not have

antibacterial properties against *E. coli*. As expected, the PMMA-HA sample also does not reveal inhibition zone (Fig. 6 (b)). It means that HA nanofibers do not possess antibacterial properties. The PMMA bone cement composite integrated with MgP nanosheets reveals an inhibition zone against *E. coli* bacteria (Fig. 6 (c)), hence indicating the antibacterial activity induced by MgP nanosheets. As reported in the earlier studies, magnesium phosphate bone cements possess antibacterial characteristics [42]. The major factor contributing to the antibacterial activity of MgP cement could be associated with its ability to induce alkalinity, which occurs due to slow and progressive dissolution of magnesium oxide (MgO) constituent into magnesium hydroxide (Mg (OH)₂) by-product, that further results into the release of hydroxyl ions

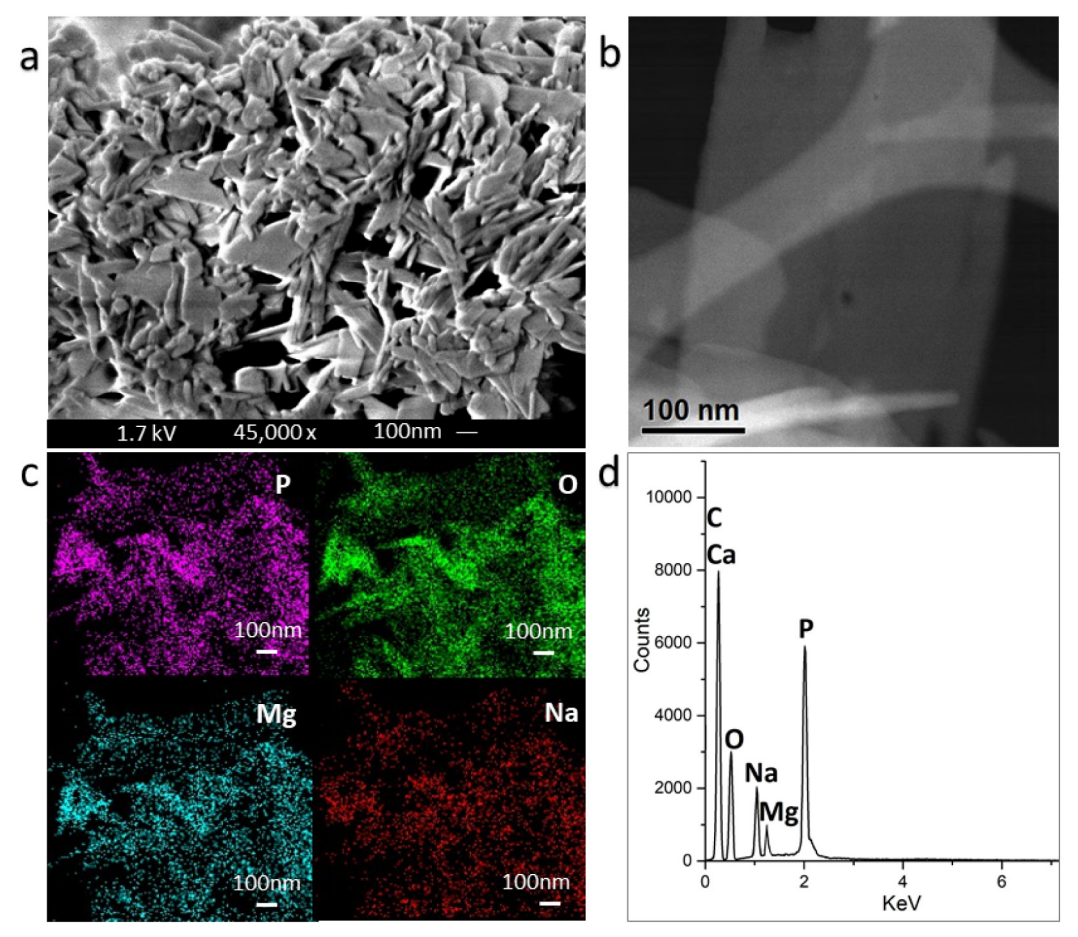


Fig. 2. Microscopy characterization of synthesized MgP nanosheets (a) FESEM image, (b) STEM image, (c) EDS in mapping mode, and (d) EDS spectra.

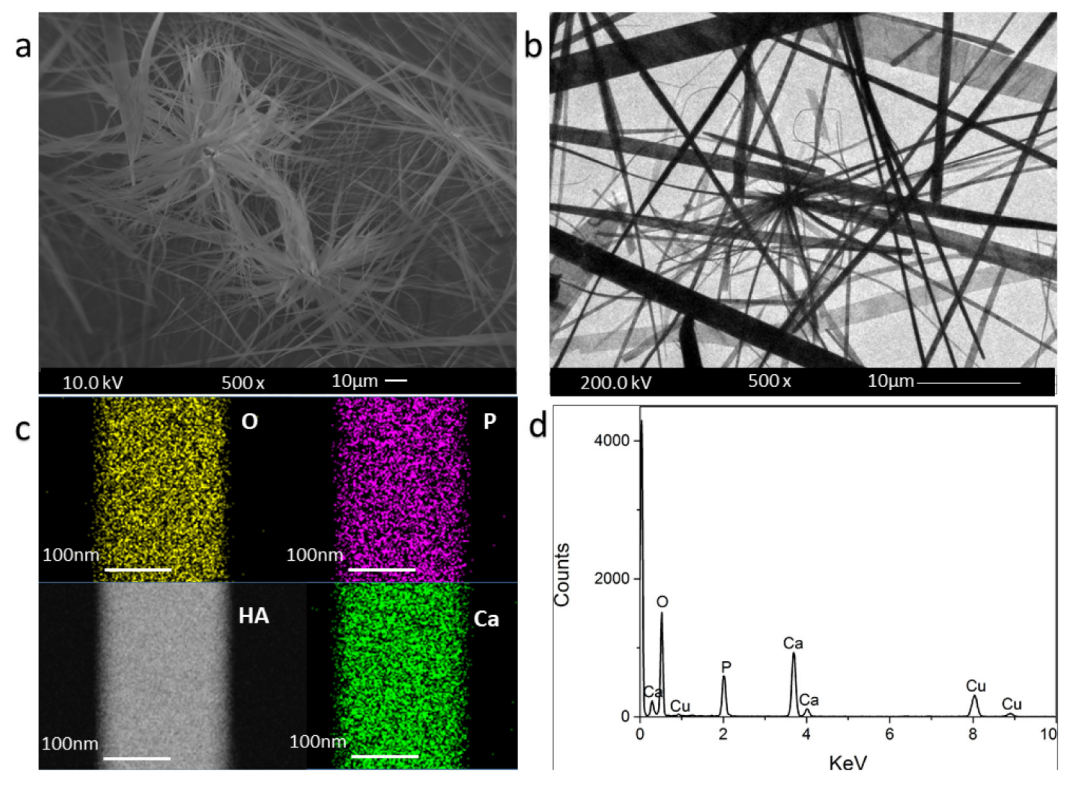


Fig. 3. Microscopy characterization of synthesized HA nanofibers: (a) FESEM image, (b) TEM image, (c) EDS spectra, and (d) EDS in mapping mode.

[42,43]. Additionally, any possible excessive release of magnesium (Mg²⁺) ions from the MgP composition matrix can inactivate bacteria due to enhanced intracellular Mg2+ ions concentrations that could eventually adversely affect riboswitch functioning and hence can possibly decrease the expression of downstream genes [44,45]. MgP composition matrix also consists of sodium (Na⁺) ions. The possible excessive release of these Na+ ions can result into the osmotic imbalance within the bacterial cells contributing to the cell death [46]. The further molecular level investigation is required to confirm various possible antibacterial mechanisms of MgP nanosheets. The antibacterial activity of various two-dimensional nanomaterials such as, graphene, graphene-oxide nanosheets, molybdenum sulfate nanosheets and phosphorene were reported to cause bacterial cell death by physical damage mechanisms. It will be interesting to investigate the ability of MgP nanosheets to cause any possible physical damage against bacterial cells [47-50]. Staphylococcus aureus (S. aureus) is the most responsible pathogen for surgical site infections [51]. Magnesium based alloys and magnesium phosphate cements have been reported to have antimicrobial resistance against S. aureus bacteria [44,52-54]. It is frequently reported that E. coli bacteria have been associated with infected implants, as well as other frequent hard tissue-related infections [55]. Therefore, MgP nanosheets can be considered as an antibacterial agent against E. coli bacteria. The PMH1, PMH2 and PMH3 nanocomposite samples also revealed an inhibition zone (Fig. 6 (d-f)). However, the biggest inhibition zone belongs to PMH1 with 7.5% wt. of MgP nanosheets. Fig. 6 (g - i) show the bacterial inhibition of all samples at different incubation times. The statistical data significance was evaluated for with One-way ANOVA followed by the Bonferroni-Holm correction for p < 0.05. The results (Fig. 6 (g-i)) indicate that PM and PMH1 bone cement composite samples have enhanced bactericidal efficiency significantly as compared with control PMMA sample after 6 h, 12 h and 24 h. Whereas the bactericidal efficiency of PMH2 and PMH3 was evaluated to significant after 12 h and 24 h of time periods. Bone cement composite sample PH shows HA nanofibers didn't exhibit bactericidal efficiency. As a whole, with the decrease of MgP

nanosheets in the matrix of nanocomposite, the inhibition zone gradually reduced.

Fig. 7 shows the results of immersion test of samples in SBF for 240 h at 37 °C. Fig. 7 (a) illustrates the schematic diagram of formation of bone like apatite on the surface of the PMMA-based nanocomposite. The changes in pH of SBF solution during 10 days of immersion are shown in Fig. 7(b). PMMA as the control sample shows a different pattern as compared to the other samples. The pH of PMMA slightly increased in the first hours of immersion likely due to the creation of OH⁻, and then the pH gradually decreased. At the initial hours (first 4 h), pH of PM, PMH, PMH1, PMH2 and PMH3 nanocomposites showed a higher pH value compared to the fresh SBF. However, the PH and PM shows the most and least increase. This initial increase in pH is possibly related to the precipitation of calcium (Ca) and phosphate (P) on the surface of the nanocomposites. Thereafter, it is illustrated that the pH of solutions decreased gradually until day 10 after the initial immersion. This reduction can be attributed to the elemental release of immersed nanocomposites. The pH of the solutions maintained between 7 and 7.17 in the last day of immersion.

Fig. 7(c) shows the surface morphology and elemental analysis of the PMM, PH, PM and PMH1 after being immersed in SBF at 37 °C for 240 h. The SEM image and EDS spectra of the PMMA sample shows spherical particles of PMMA with no deposition of calcium phosphate on the surface. This confirms that PMMA is not bioactive [56]. The incorporation of MgP nanosheets into PMMA matrix leads to the partially formation of the apatite on the surface of the sample. This indicates that magnesium phosphate nanosheets increase the bioactivity of samples [57]. As shown in Figure the apatite layer became increasingly thicker on PH surface as compared with the PM surface, suggesting that the introduction of HA to the PMMA could further increase the bioactivity level of the surface [58]. In addition, mineralization on the surface of the PMH1 sample was similar to that on surface of PH sample. These features show that the PMH composite possibly induce the bone-like apatite nucleation and growth on their surfaces from SBF. It was reported that bone-like apatite layer is important to establish the

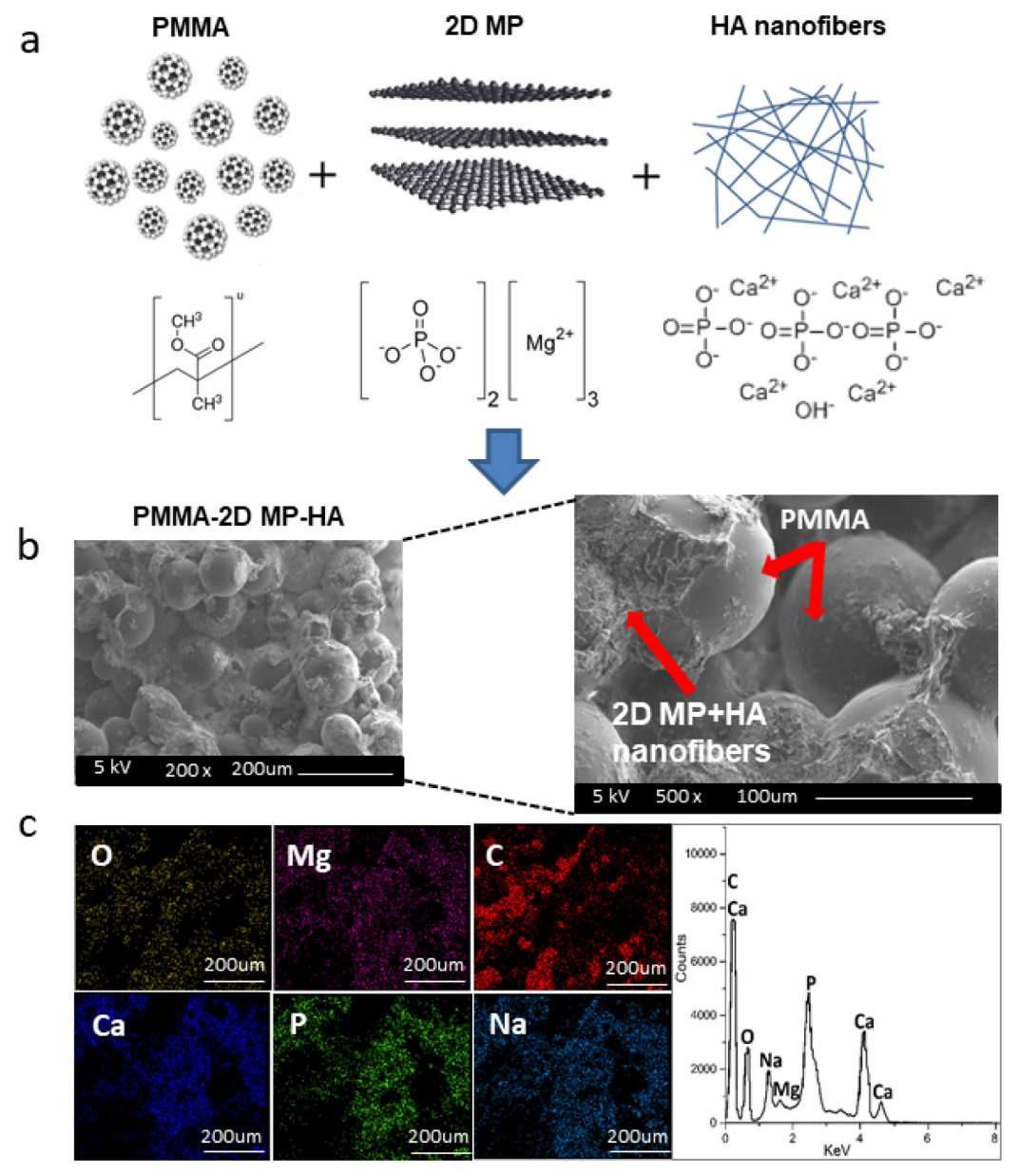


Fig. 4. PMMA-MgP-HA nanocomposite (a) Schematic diagram for the formation of nanocomposite (b) SEM images in two different magnifications (c) EDS mapping of with PMMA-MgP-HA nanocomposite with EDS spectrum.

bone-bonding interface between bioactive materials and living tissues [59].

Fig. 8 shows a comparative cytotoxic result between P, PM, PH, PMH1, PMH2, and PMH3 samples obtained though MTT assay. Fig. 8 (a-g) illustrates the optical microcopy of the cells at different density, and Fig. 8 (h) represents the absorptions at 570 nm wavelength. The results indicate that the cytotoxicity of cells exposed to P specimen for 24 h are higher than other samples. Incorporation of magnesium phosphate to PMMA matrix reduces the cytotoxicity of nanocomposite. This is related to the similar biological properties of the magnesium phosphate to calcium phosphate and its low level of cytotoxicity [34]. Possible release of magnesium (Mg²⁺) ions helps in DNA stabilization and in the regulation of sodium and calcium ions channels [35,36]. The lowest level of cytotoxicity belongs to the PH composite with the 10 wt % of HA nanofibers. This is possibly due to the existence of HA nanofibers that can release Ca2+ ions which are essential for cellular functions and hence possibly responsible for enhanced cells proliferation [60]. This result is in close agreement with the finding of Zhang et al.

[61]. Overall, there is no significant difference in cytotoxicity of PMH1, PMH2 and PMH3. However, with the decrease of HA nanofiber in the composite, the amount of cytotoxicity slightly increased. Therefore, the incorporation of either HA nanofibers or MgP nanosheets into the PMMA matrix increases the cell viability of the composite and consequently reduce the cytotoxicity of the PMMA. Fig. 8 (h) illustrates the quantity of fibroblast cells exposed to the samples for 24 h. The statistical data significance was evaluated for with One-way ANOVA followed by the Bonferroni-Holm correction for p < 0.05. The results (Fig. 8(h)) show that significant reduction in the cell viability was observed in bone cement composite P, PM, PMH1, PMH2, PMH3 samples as compared with positive Control sample. Whereas bone cement composite sample PH displayed enhanced cellular viability than sample P and no significant difference as compared with positive control sample. It reveals that more cells survived in the order of PH > PMH1 > PMH2 > PMH3 > PM > P. Further in-vivo studies need to be investigated for more understanding of the cytocompatibility of PMMA-MgP-HA bone cement nanocomposites. In addition to the

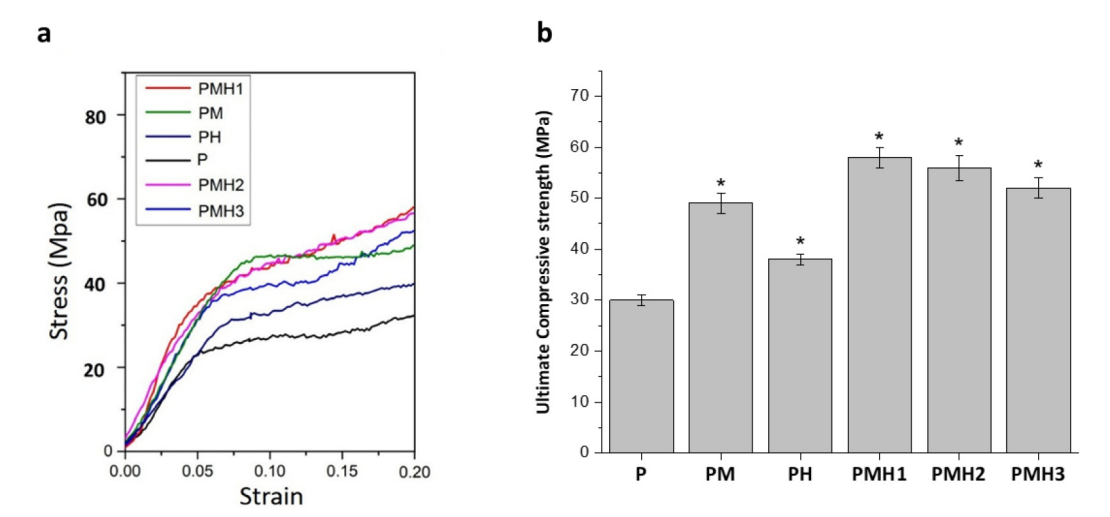


Fig. 5. Compression strength for P, PH, PM, PMH1, PMH2 and PMH3 nanocomposite samples: (a) stress vs. strain curve, and (b) ultimate compressive strength. The error bars represent \pm standard deviation for n=3. *, p<0.05 evaluated as statistically significant for all other PMMA bone cement composite samples (PM, PH, PMH1, PMH2, PMH3) as compared with PMMA control (P) sample after Bonferroni-Holm's correction.

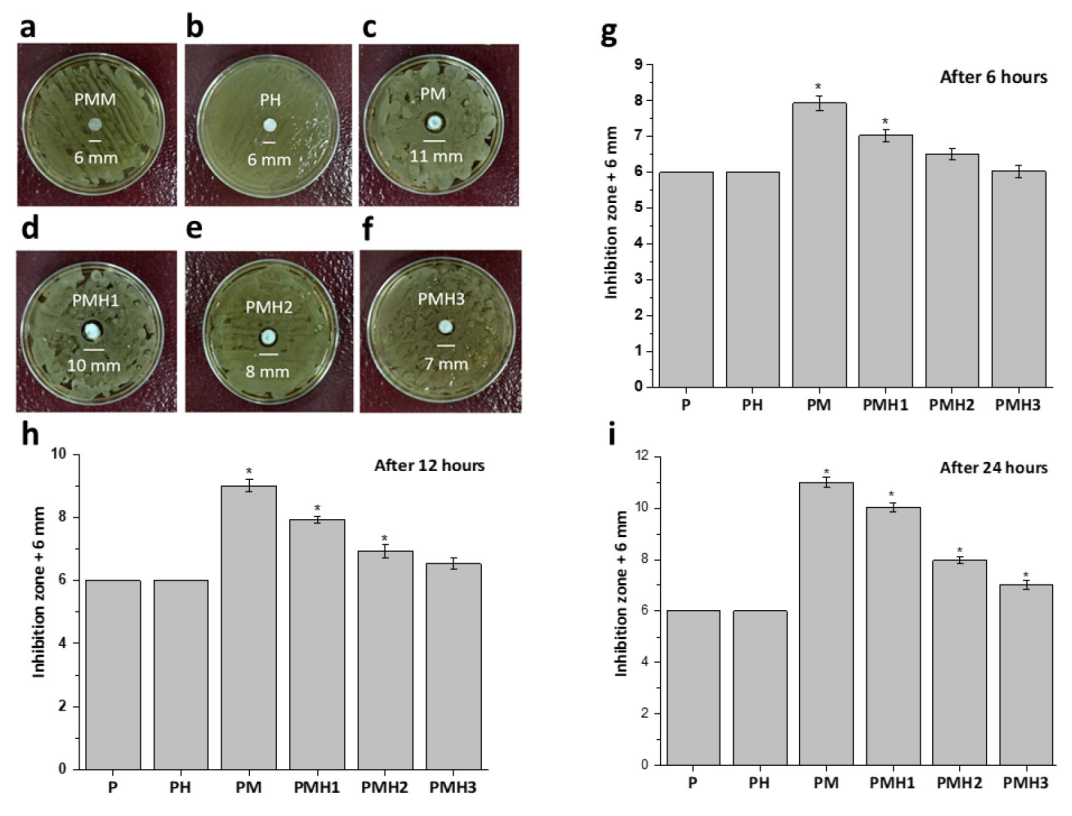


Fig. 6. Antibacterial activity of control and nanocomposite samples with different ratios against *E. coli*. bacteria (a-f) inhibition zone of control and nanocomposite samples (g) inhibition zone of samples after 6 h of incubation time (h) inhibition zone of samples after 12 h of incubation time (i) inhibition zone of samples after 24 h of incubation time. The error bars represent \pm standard deviation for n = 3. *, p < 0.05 evaluated as statistically significant for PMMA bone cement composite samples (PM, PH, PMH1, PMH2, PMH3) as compared with PMMA control (P) sample after Bonferroni-Holm's correction. Otherwise P > 0.05 indicates absence of *.

bioactivity and cytotoxicity evaluations of PMMA-MgP-HA bone cement composites, further molecular level polymerase chain reaction (PCR) investigations of fibroblast cells can provide details of gene expressions which can be ultimately correlated with altered cellular metabolism due to MgP nanosheets and HA nanofibers constituents.

4. Conclusion

In the present work, two-dimensional magnesium phosphate

nanosheets and one-dimensional hydroxyapatite nanofibers were synthesized by tuning the crystallization of the sodium-magnesium-phosphate ternary system and hydrothermal homogeneous precipitation, respectively. A novel PMMA bone cement nanocomposite was then developed by mixing magnesium phosphate nanosheets and HA nanofibers in different ratios. The results reveal that the incorporation of MgP nanosheets into the PMMA matrix leads to increase in the antibacterial properties of the PMMA bone cement composite against *E. coli* bacteria. In addition, both MgP nanosheets and HA nanofiber improve

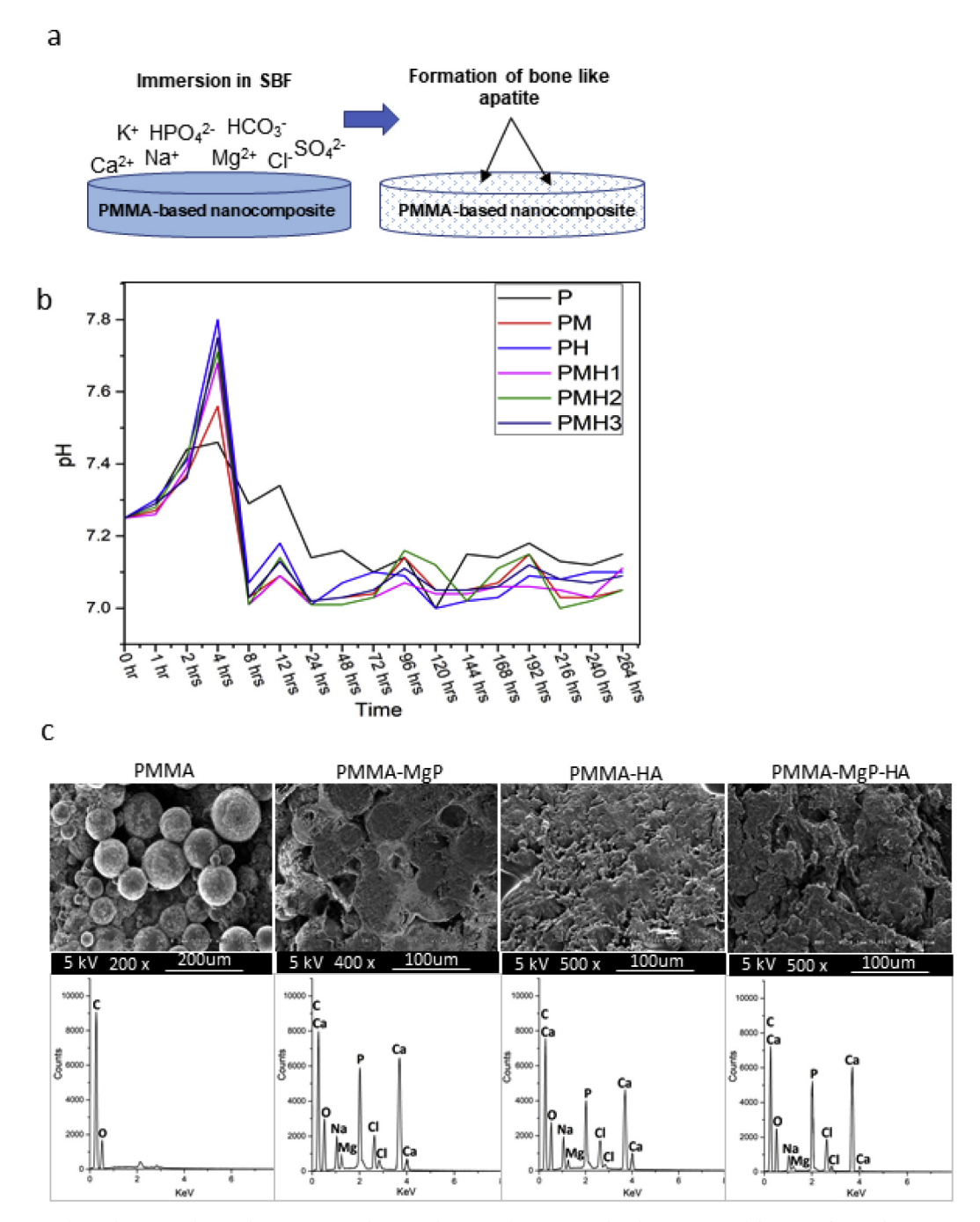


Fig. 7. Immersion test of samples in SBF for 240 h at 37 $^{\circ}$ C (a) Schematic diagram of immersion (b) Change in pH of the SBF solution during immersion (c) SEM and EDS spectrum of PMMA, PM, PH, PMH1 after immersion test (NOTE: n = 3; data shown as mean).

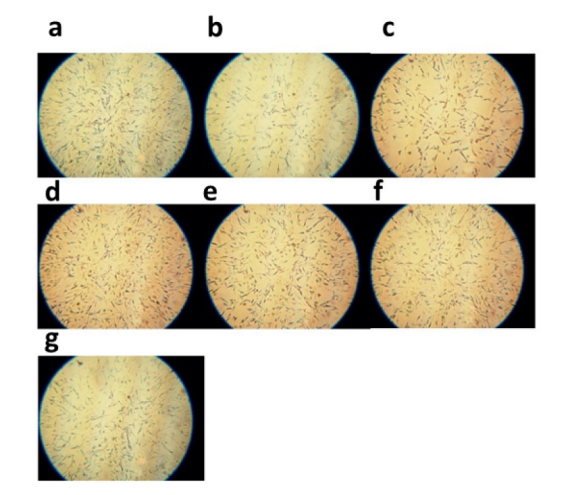
the compression strength of the bone cement nanocomposite, however, the effect of MgP nanosheets is more significant. The results, therefore, demonstrate that the highest ultimate compression strength belongs to the nanocomposite with 7.5 wt% magnesium phosphate nanosheets and 2.5 wt% HA nanofibers. Immersion test in SBF reveals that both additives increased the bioactivity of the bone cements. Finally, MTT assay results indicate that PMMA as a control sample has the lowest cytocompatibility, however, PMMA-MgP with 10 wt% magnesium phosphate nanosheets has the highest amount of cytocompatibility. Thus, the current study suggests that MgP nanosheets and HA nanofibers can be considered as potential filler components for the next generation of PMMA bone cement nanocomposites.

Declaration of competing interest

The authors declare no conflict of interests.

Acknowledgement

T. Shokuhfar is grateful to the NSF-CBET Award number 1803693. R. Shahbazian-Yassar acknowledges the financial support from NSF-DMR Award number 1710049. TEM imaging work made use of instruments in the Electron Microscopy Service (Research Resources Center, UIC).



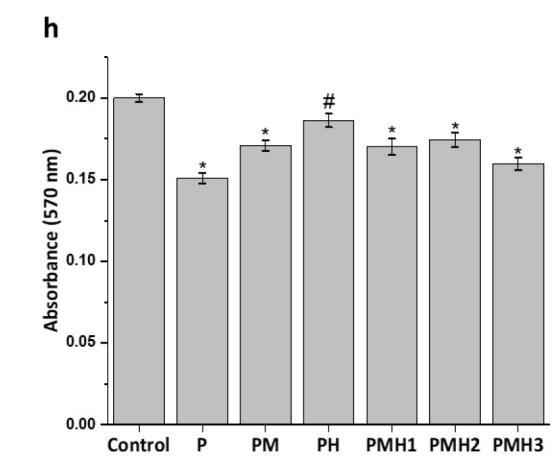


Fig. 8. Cytotoxicity results (a-g) optical microscopy and (h) MTT absorbance of the control, P, PM, PH, PMH1, PMH2, and PMH3 samples after 24 h of MTT assay. The error bars represent \pm standard deviation for n=3. *, p<0.05 evaluated as statistically significant for all other PMMA bone cement composite samples (P, PM, PMH1, PMH2, PMH3) except sample PH as compared with positive control (Control) sample after Bonferroni-Holm's correction. #, P<0.05 evaluated as statistically significant between PMMA control (P) sample and (PH) sample after Bonferroni-Holm's correction. P>0.05 for PMMA bone cement composites (PM, PMH1, PMH2, PMH3) groups as compared with control PMMA (P) group as evaluated with One-way ANOVA technique.

References

- [1] K. Anusavice, R.P.-S.L.W. Saunders, Science of Dental Materials, (2003).
- [2] Z. Sayeed, M.T. Padela, M.M. El-Othmani, K.J. Saleh, Acrylic bone cements for joint replacement, Biomed. Compos, Elsevier, 2017, pp. 199–214, https://doi.org/10. 1016/B978-0-08-100752-5.00009-3.
- [3] D. Çökeliler, S. Erkut, J. Zemek, H. Biederman, M. Mutlu, Modification of glass fibers to improve reinforcement: a plasma polymerization technique, Dent. Mater. 23 (2007) 335–342, https://doi.org/10.1016/j.dental.2006.01.023.
- [4] G. Lazouzi, M.M. Vuksanović, N.Z. Tomić, M. Mitrić, M. Petrović, V. Radojević, R.J. Heinemann, Optimized preparation of alumina based fillers for tuning composite properties, Ceram. Int. 44 (2018) 7442–7449, https://doi.org/10.1016/j. ceramit 2018.01.083
- [5] H.-J. Jiang, J. Xu, Z.-Y. Qiu, X.-L. Ma, Z.-Q. Zhang, X.-X. Tan, Y. Cui, F.-Z. Cui, Editor, A.A. Zadpoor, Mechanical properties and cytocompatibility improvement of vertebroplasty PMMA bone cements by incorporating mineralized collagen, Materials (Basel). 8 (2015) 2616–2634. doi:https://doi.org/10.3390/ma8052616.
- [6] J. Han, G. Ma, J. Nie, A facile fabrication of porous PMMA as a potential bone substitute, Mater. Sci. Eng. C. 31 (2011) 1278–1284, https://doi.org/10.1016/j. poroc. 2011.04.001
- [7] S.B. Kim, Y.J. Kim, T.L. Yoon, S.A. Park, I.H. Cho, E.J. Kim, I.A. Kim, J.-W. Shin, The characteristics of a hydroxyapatite-chitosan-PMMA bone cement, Biomaterials 25 (2004) 5715–5723, https://doi.org/10.1016/j.biomaterials.2004.01.022.
- [8] M. Arora, Polymethylmethacrylate bone cements and additives: a review of the literature, World J. Orthop. 4 (2013) 67, https://doi.org/10.5312/wjo.v4.i2.67.
- [9] S. Aghyarian, E. Bentley, T.N. Hoang, I.M. Gindri, V. Kosmopoulos, H.K.W. Kim, D.C. Rodrigues, In vitro and in vivo characterization of premixed PMMA-CaP composite bone cements, ACS Biomater. Sci. Eng. 3 (2017) 2267–2277, https://doi. org/10.1021/acsbiomaterials.7b00276.
- [10] A. Sugino, T. Miyazaki, G. Kawachi, K. Kikuta, C. Ohtsuki, Relationship between apatite-forming ability and mechanical properties of bioactive PMMA-based bone cement modified with calcium salts and alkoxysilane, J. Mater. Sci. Mater. Med. 19 (2008) 1399–1405, https://doi.org/10.1007/s10856-007-3257-5.
- [11] M.R. Ayatollahi, M.Y. Yahya, H. Asgharzadeh Shirazi, S.A. Hassan, Mechanical and tribological properties of hydroxyapatite nanoparticles extracted from natural bovine bone and the bone cement developed by nano-sized bovine hydroxyapatite filler, Ceram. Int. 41 (2015) 10818–10827, https://doi.org/10.1016/j.ceramint. 2015.05.021.
- [12] K.A. Mann, M.A. Miller, R.J. Cleary, D. Janssen, N. Verdonschot, Experimental micromechanics of the cement-bone interface, J. Orthop. Res. 26 (2008) 872–879, https://doi.org/10.1002/jor.20575.
- [13] S.Y. Kwon, Y.S. Kim, Y.K. Woo, S.S. Kim, J.B. Park, Hydroxyapatite impregnated bone cement: in vitro and in vivo studies, Biomed. Mater. Eng. 7 (1997) 129–140, https://doi.org/10.3233/BME-1997-7205.
- [14] M.L. Qi, Z. Huang, W. Yao, F. Long, M. Cheng, B. Song, D. Banner, R. Shahbazian-Yassar, Y.P. Lu, T. Shokuhfar, In situ visualization of the superior nanomechanical flexibility of individual hydroxyapatite nanobelts, CrystEngComm 20 (2018) 1031–1036, https://doi.org/10.1039/c7ce01852e.
- [15] A.M. Moursi, A.V. Winnard, P.L. Winnard, J.J. Lannutti, R.R. Seghi, Enhanced osteoblast response to a polymethylmethacrylate-hydroxyapatite composite, Biomaterials 23 (2002) 133–144, https://doi.org/10.1016/S0142-9612(01) 00088-6.
- [16] F.A. Alzarrug, M.M. Dimitrijević, R.M. Jančić Heinemann, V. Radojević, D.B. Stojanović, P.S. Uskoković, R. Aleksić, The use of different alumina fillers for improvement of the mechanical properties of hybrid PMMA composites, Mater. Des.

- 86 (2015) 575-581, https://doi.org/10.1016/j.matdes.2015.07.069.
- [17] E. Paz, F. Forriol, J.C. del Real, N. Dunne, Graphene oxide versus graphene for optimisation of PMMA bone cement for orthopaedic applications, Mater. Sci. Eng. C. 77 (2017) 1003–1011, https://doi.org/10.1016/j.msec.2017.03.269.
- [18] R. Ormsby, T. McNally, C. Mitchell, N. Dunne, Incorporation of multiwalled carbon nanotubes to acrylic based bone cements: effects on mechanical and thermal properties, J. Mech. Behav. Biomed. Mater. 3 (2010) 136–145, https://doi.org/10. 1016/j.jmbbm.2009.10.002.
- [19] M.K. Singh, T. Shokuhfar, J.J. De Almeida Gracio, A.C.M. De Sousa, J.M. Da Fonte Fereira, H. Garmestani, S. Ahzi, Hydroxyapatite modified with carbon-nanotubereinforced poly(methyl methacrylate): a nanocomposite material for biomedical applications, Adv. Funct. Mater. 18 (2008) 694–700, https://doi.org/10.1002/ adfm.200700888.
- [20] J. Hill, J. Orr, N. Dunne, In vitro study investigating the mechanical properties of acrylic bone cement containing calcium carbonate nanoparticles, J. Mater. Sci. Mater. Med. 19 (2008) 3327–3333, https://doi.org/10.1007/s10856-008-3465-7.
- [21] J. Slane, J. Vivanco, J. Meyer, H.L. Ploeg, M. Squire, Modification of acrylic bone cement with mesoporous silica nanoparticles: effects on mechanical, fatigue and absorption properties, J. Mech. Behav. Biomed. Mater. 29 (2014) 451–461, https:// doi.org/10.1016/j.jmbbm.2013.10.008.
- [22] A. Gutiérrez-Mejía, W. Herrera-Kao, S. Duarte-Aranda, M.I. Loría-Bastarrachea, G. Canché-Escamilla, F.J. Moscoso-Sánchez, J.V. Cauich-Rodríguez, J.M. Cervantes-Uc, Synthesis and characterization of core-shell nanoparticles and their influence on the mechanical behavior of acrylic bone cements, Mater. Sci. Eng. C. 33 (2013) 1737–1743, https://doi.org/10.1016/j.msec.2012.12.087.
- [23] W. Yu, X. Wang, Q. Tang, M. Guo, J. Zhao, Reinforcement of denture base PMMA with ZrO 2 nanotubes, J. Mech. Behav. Biomed. Mater. 32 (2014) 192–197, https:// doi.org/10.1016/j.jmbbm.2014.01.003.
- [24] J. Slane, J. Vivanco, W. Rose, H.L. Ploeg, M. Squire, Mechanical, material, and antimicrobial properties of acrylic bone cement impregnated with silver nanoparticles, Mater. Sci. Eng. C. 48 (2015) 188–196, https://doi.org/10.1016/j.msec. 2014.11.068.
- [25] E. Bertazzoni Minelli, T. Della Bora, A. Benini, Different microbial biofilm formation on polymethylmethacrylate (PMMA) bone cement loaded with gentamicin and vancomycin, Anaerobe 17 (2011) 380–383, https://doi.org/10.1016/j.anaerobe. 2011.03.013.
- [26] V. Alt, T. Bechert, P. Steinrücke, M. Wagener, P. Seidel, E. Dingeldein, E. Domann, R. Schnettler, An in vitro assessment of the antibacterial properties and cytotoxicity of nanoparticulate silver bone cement, Biomaterials 25 (2004) 4383–4391, https:// doi.org/10.1016/i.biomaterials.2003.10.078.
- 27] T. Russo, A. Gloria, R. De Santis, U. D'Amora, G. Balato, A. Vollaro, O. Oliviero, G. Improta, M. Triassi, L. Ambrosio, Preliminary focus on the mechanical and antibacterial activity of a PMMA-based bone cement loaded with gold nanoparticles, Bioact. Mater. 2 (2017) 156–161, https://doi.org/10.1016/j.bioactmat.2017.05.002.
- [28] P.E. Petrochenko, J. Zheng, B.J. Casey, M.R. Bayati, R.J. Narayan, P.L. Goering, Nanosilver-PMMA composite coating optimized to provide robust antibacterial efficacy while minimizing human bone marrow stromal cell toxicity, Toxicol. Vitr. 44 (2017) 248–255, https://doi.org/10.1016/j.tiv.2017.07.014.
- [29] H. Kong, J. Jang, Antibacterial properties of novel poly(methyl methacrylate) nanofiber containing silver nanoparticles, Langmuir 24 (2008) 2051–2056, https:// doi.org/10.1021/la703085e.
- [30] A. Barbasz, M. Oćwieja, M. Roman, Toxicity of silver nanoparticles towards tumoral human cell lines U-937 and HL-60, Colloids Surfaces B Biointerfaces 156 (2017) 397–404, https://doi.org/10.1016/j.colsurfb.2017.05.027.

- [31] Y.P. Jia, B.Y. Ma, X.W. Wei, Z.Y. Qian, The in vitro and in vivo toxicity of gold nanoparticles, Chinese Chem. Lett. 28 (2017) 691–702, https://doi.org/10.1016/j. cclet.2017.01.021.
- [32] S.R. Shah, A.M. Tatara, J. Lam, S. Lu, D.W. Scott, G.N. Bennett, J.J.J.P. Van Den Beucken, J.A. Jansen, M.E. Wong, A.G. Mikos, Polymer-based local antibiotic delivery for prevention of polymicrobial infection in contaminated mandibular implants, ACS Biomater. Sci. Eng. 2 (2016) 558–566, https://doi.org/10.1021/ acsbiomaterials.5b00545.
- [33] J.H. Lee, J.K. Jo, D.A. Kim, K.D. Patel, H.W. Kim, H.H. Lee, Nano-graphene oxide incorporated into PMMA resin to prevent microbial adhesion, Dent. Mater. 34 (2018) e63–e72, https://doi.org/10.1016/j.dental.2018.01.019.
- [34] F. Tamimi, D. Le Nihouannen, D.C. Bassett, S. Ibasco, U. Gbureck, J. Knowles, A. Wright, A. Flynn, S.V. Komarova, J.E. Barralet, Biocompatibility of magnesium phosphate minerals and their stability under physiological conditions, Acta Biomater. 7 (2011) 2678–2685, https://doi.org/10.1016/j.actbio.2011.02.007.
- [35] F.I. Wolf, V. Trapani, Cell (patho)physiology of magnesium, Clin. Sci. 114 (2008) 27–35, https://doi.org/10.1042/CS20070129.
- [36] M. Nabiyouni, T. Brückner, H. Zhou, U. Gbureck, S.B. Bhaduri, Magnesium-based bioceramics in orthopedic applications, Acta Biomater. 66 (2018) 23–43, https://doi.org/10.1016/j.actbio.2017.11.033.
- [37] M. Laurenti, A. Al Subaie, M.N. Abdallah, A.R.G. Cortes, J.L. Ackerman, H. Vali, K. Basu, Y.L. Zhang, M. Murshed, S. Strandman, J. Zhu, N. Makhoul, J.E. Barralet, F. Tamimi, Two-dimensional magnesium phosphate nanosheets form highly thix-otropic gels that up-regulate bone formation, Nano Lett. 16 (2016) 4779–4787, https://doi.org/10.1021/acs.nanolett.6b00636.
- [38] M.L. Qi, Z. Huang, A. Phakatkar, W. Yao, Y. Yuan, T. Foroozan, G.Y. Xiao, R. Shahbazian-Yassar, Y.P. Lu, T. Shokuhfar, Facile hydrothermal synthesis of antibacterial multi-layered hydroxyapatite nanostructures with superior flexibility, CrystEngComm 20 (2018) 1304–1312, https://doi.org/10.1039/c7ce01938f.
- [39] ISO I, 5833 implants for surgery–acrylic resin cements, Geneva Int. Test. Organ.
 (2002)
- [40] M. Rezazadeh Shirdar, I. Sudin, M.M. Taheri, A. Keyvanfar, M.Z.M. Yusop, M.R.A. Kadir, A novel hydroxyapatite composite reinforced with titanium nanotubes coated on Co-Cr-based alloy, Vacuum. 122 (2015) 82–89, https://doi.org/10. 1016/j.vacuum.2015.09.008.
- [41] M. Arora, E.K.S. Chan, S. Gupta, A.D. Diwan, Polymethylmethacrylate bone cements and additives: a review of the literature, World J. Orthop. 4 (2013) 67–74, https://doi.org/10.5312/wjo.v4.i2.67.
- [42] G. Mestres, M.P. Ginebra, Novel magnesium phosphate cements with high early strength and antibacterial properties, Acta Biomater. 7 (2011) 1853–1861, https://doi.org/10.1016/j.actbio.2010.12.008.
- [43] E. Soudée, J. Péra, Mechanism of setting reaction in magnesia-phosphate cements, Cem. Concr. Res. 30 (2000) 315–321, https://doi.org/10.1016/S0008-8846(99) 00254-9.
- [44] H. Feng, G. Wang, W. Jin, X. Zhang, Y. Huang, A. Gao, H. Wu, G. Wu, P.K. Chu, Systematic study of inherent antibacterial properties of magnesium-based biomaterials, ACS Appl. Mater. Interfaces 8 (2016) 9662–9673, https://doi.org/10.1021/ acsami.6b02241
- [45] C.E. Dann, C.A. Wakeman, C.L. Sieling, S.C. Baker, I. Irnov, W.C. Winkler, Structure and mechanism of a metal-sensing regulatory RNA, Cell 130 (2007) 878–892, https://doi.org/10.1016/j.cell.2007.06.051.
- [46] S. Yadav, J.P. Yadav, Antimicrobial activity of Cassia occidentalis L (leaf) against various human pathogenic microbes, http://astonjournals.com/lsmr, (2010), Accessed date: 18 October 2019.

- [47] F. Alimohammadi, M. Sharifian, N.H. Attanayake, A.C. Thenuwara, Y. Gogotsi, B. Anasori, D.R. Strongin, Antimicrobial properties of 2D MnO 2 and MoS 2 Nanomaterials vertically aligned on graphene materials and Ti 3 C 2 MXene, Langmuir 34 (2018) 7192–7200, https://doi.org/10.1021/acs.langmuir.8b00262.
- [48] Z. Xiong, X. Zhang, S. Zhang, L. Lei, W. Ma, D. Li, W. Wang, Q. Zhao, B. Xing, Bacterial toxicity of exfoliated black phosphorus nanosheets, Ecotoxicol. Environ. Saf. 161 (2018) 507–514, https://doi.org/10.1016/j.ecoenv.2018.06.008.
- [49] S.S. Nanda, D.K. Yi, K. Kim, Study of antibacterial mechanism of graphene oxide using Raman spectroscopy, Sci. Rep. 6 (2016), https://doi.org/10.1038/srep28443.
- [50] Y. Tu, M. Lv, P. Xiu, T. Huynh, M. Zhang, M. Castelli, Z. Liu, Q. Huang, C. Fan, H. Fang, R. Zhou, Destructive extraction of phospholipids from *Escherichia coli* membranes by graphene nanosheets, Nat. Nanotechnol. 8 (2013) 594–601, https://doi.org/10.1038/nnano.2013.125.
- [51] H. Humphreys, K. Becker, P.M. Dohmen, N. Petrosillo, M. Spencer, M. van Rijen, A. Wechsler-Fördös, M. Pujol, A. Dubouix, J. Garau, Staphylococcus aureus and surgical site infections: benefits of screening and decolonization before surgery, J. Hosp. Infect. 94 (2016) 295–304, https://doi.org/10.1016/j.jhin.2016.06.011.
- [52] J. Sawai, H. Kojima, H. Igarashi, A. Hashimoto, S. Shoji, T. Sawaki, A. Hakoda, E. Kawada, T. Kokugan, M. Shimizu, Antibacterial characteristics of magnesium oxide powder, World J. Microbiol. Biotechnol. 16 (2000) 187–194, https://doi.org/ 10.1023/A:1008916209784.
- [53] D.A. Robinson, R.W. Griffith, D. Shechtman, R.B. Evans, M.G. Conzemius, In vitro antibacterial properties of magnesium metal against *Escherichia coli*, Pseudomonas aeruginosa and Staphylococcus aureus, Acta Biomater. 6 (2010) 1869–1877, https://doi.org/10.1016/j.actbio.2009.10.007.
- [54] Y. Zhou, C. Xu, X. Wang, Y. Dou, Z. Huan, J. Chang, Fast setting tricalcium silicate/magnesium phosphate premixed cement for root canal filling, Ceram. Int. 44 (2018) 3015–3023, https://doi.org/10.1016/j.ceramint.2017.11.058.
- [55] G. Mestres, M. Abdolhosseini, W. Bowles, S.H. Huang, C. Aparicio, S.U. Gorr, M.P. Ginebra, Antimicrobial properties and dentin bonding strength of magnesium phosphate cements, Acta Biomater. 9 (2013) 8384–8393, https://doi.org/10.1016/ i.actbio.2013.05.032.
- [56] T. Kang, X. Hua, P. Liang, M. Rao, Q. Wang, C. Quan, C. Zhang, Q. Jiang, Synergistic reinforcement of polydopamine-coated hydroxyapatite and BMP2 biomimetic peptide on the bioactivity of PMMA-based cement, Compos. Sci. Technol. 123 (2016) 232–240, https://doi.org/10.1016/j.compscitech.2016.01.002.
- [57] G. Yang, J. Liu, F. Li, Z. Pan, X. Ni, Y. Shen, H. Xu, Q. Huang, Bioactive calcium sulfate/magnesium phosphate cement for bone substitute applications, Mater. Sci. Eng. C. 35 (2014) 70–76, https://doi.org/10.1016/j.msec.2013.10.016.
- [58] G. Radha, S. Balakumar, B. Venkatesan, E. Vellaichamy, A novel nano-hydroxyapatite — PMMA hybrid scaffolds adopted by conjugated thermal induced phase separation (TIPS) and wet-chemical approach: analysis of its mechanical and biological properties, Mater. Sci. Eng. C. 75 (2017) 221–228, https://doi.org/10.1016/ i.msec.2016.12.133.
- [59] Y.W. Gu, K.A. Khor, P. Cheang, In vitro studies of plasma-sprayed hydroxyapatite/ Ti-6Al-4V composite coatings in simulated body fluid (SBF), Biomaterials 24 (2003) 1603–1611, https://doi.org/10.1016/S0142-9612(02)00573-2.
- [60] X. Yang, Y. Li, X. Liu, R. Zhang, Q. Feng, In Vitro Uptake of Hydroxyapatite Nanoparticles and Their Effect on Osteogenic Differentiation of Human Mesenchymal Stem Cells, (2018), https://doi.org/10.1155/2018/2036176.
- [61] J. Zhang, A. Mo, J. Li, X. Wang, Y. Li, Characteristics of hydroxyapatite/PMMA nanocomposites for provisional restoration and its biocompatibility with human gingival fibroblasts, J. Sichuan Univ. Med. Sci. Ed. 45 (2014) 502–505.